



Monitoring snowmelt induced unsaturated flow and transport using electrical resistivity tomography

Helen K. French^{*}, Carol Hardbattle^b, Andrew Binley^b, Peter Winship^b, Leif Jakobsen^a

^a*Department of Soil and Water Sciences, The Agricultural University of Norway, P.O. Box 5028, 1432 Ås, Norway*

^b*Department of Environmental Science, Lancaster University, Lancaster LA1 4YQ, UK*

Abstract

The flow and transport of a non-reactive tracer and melt water was monitored in a heterogeneous coarse sandy unsaturated zone in southeastern Norway, during the snowmelt of 2001. Electrical resistivity tomography (ERT) as well as conventional suction cup techniques was employed. A frozen solution of NaBr in water was supplied as a line source on the ground surface above two parallel vertical profiles monitored by the two measurement systems prior to the onset of snowmelt. The two monitored vertical profiles were separated by approximately 1 m. The results were analysed by visual comparison of images and by the use of spatial moments analysis. The two measurement approaches showed that the system was affected by the presence of preferential flow paths during the early stages of the snowmelt, perhaps due to ice near the surface, but the major part of the plume moves uniformly later in the snow-melting period. After most of the tracer plume has reached the depth monitored by both systems (i.e. below 0.4 m depth) there is a good consistency between the two datasets. Spatial moment calculations on the basis of ERT cannot be used to describe the movement of tracer alone, as the resistivity is affected by changes in both saturation levels and tracer concentration. Nevertheless, ERT appears to be an appropriate method to characterise regions of localised high infiltration in this type of soil. The method therefore constitutes a possible alternative and supplement to suction cups in a monitoring system. © 2002 Elsevier Science B.V. All rights reserved.

Keywords: Snowmelt; Tracers; Electrical resistivity tomography; Lysimeter

1. Introduction

Oslo airport, Gardermoen, is situated on Norway's largest unconfined aquifer, which consists of coarse sandy sediments. It is during snowmelt and after heavy rains that the risk of pollution of the ground water caused by airport operations is the greatest. The horizontal distribution of ground frost and basal ice can cause focused infiltration, which in turn can influence the retention time in the unsaturated zone. Because of climatic conditions, de-icing chemicals have the greatest potential for polluting the local

groundwater, due to the large volumes used during winter and the danger of focused infiltration during snowmelt. Understanding and monitoring flow and transport in the unsaturated zone is therefore important.

Monitoring the pollution from a large area is a major challenge. Oslo airport, for instance, has a total of 60 suction cups, of the same type used in the experiments described here and earlier (French et al., 1999), for monitoring the unsaturated zone along the side of the two runways and the de-icing platform (all in all equivalent to a plan area of several thousand square metres). Geophysical methods may provide a useful supplement or alternative to the more common suction cup technique. The geophysical method

^{*} Corresponding author. Fax: +47-649-48211.

E-mail address: helen.french@ijvf.nlh.no (H.K. French).

selected for our experiment is cross-borehole electrical resistivity tomography (ERT) (Daily et al., 1992; Slater et al., 2000). In our set-up the technique provides two-dimensional images of the resistivity distribution in a vertical section of the unsaturated zone. The advantage of ERT compared to suction cups, is that the electrodes are relatively easy to install and are inexpensive. Labour costs are also significantly less than those for analysis of water samples and with the wide availability of remote monitoring data acquisitions systems, labour costs are likely to be significantly reduced in the future.

The measured resistances are functions of soil structure, water content and pore water electrical conductivity. In a melting partly frozen soil, water contents will change because of infiltrating melt water, the unfrozen water content will change due to melting and the infiltration of an electrolytic tracer will increase the conductivity of the soil water. In the literature, the success of a number of electric, electromagnetic and seismo-acoustic techniques for determination of the distribution and properties of permafrost has been reported (Scott et al., 1978; Arcone et al., 1979; Sinha and Stephens, 1983; Todd and Dallimore, 1998; Stein and Kane, 1983).

A field site at Moreppen has been constructed to characterise the early infiltration and flow during snowmelt through the unsaturated zone, which consists of heterogeneous coarse sandy soil, by employing ERT together with more conventional techniques. Unsaturated flow and transport during snowmelt have previously been, and were together with ERT in 2001, monitored at Moreppen by the use of suction cups (French et al., 1994; French et al., 1999). By combining geophysical and hydrological techniques at the same site, our objective is to quantify the consistency in the different field measurement techniques and to examine whether ERT could serve as a valuable supplement or replacement in monitoring systems for such an environment.

2. Experimental method

2.1. The field site

The fieldwork for this experiment was carried out next to a lysimeter trench at Moreppen, Gardermoen

(French et al., 1994) in southeastern Norway (Fig. 1). The Gardermoen glacial-contact delta is an aquifer composed of sand and gravel underlain by silty glaciomarine deposits (Jørgensen and Østmo, 1990; Tuttle, 1997). The unsaturated zone (1–30 m thick) is heterogeneous, with sediments of fine to coarse sand and gravel. In its natural state, the ground surface is mostly forested (mainly spruce) with open areas of pioneer vegetation (grass, bushes, young birch). The annual precipitation is approximately 800 mm and the evapotranspiration is about 400 mm. More than 50% of the groundwater recharge occurs during the snowmelt period (3–5 weeks) (Jørgensen and Østmo, 1990). The unsaturated zone at the field site mainly consists of coarse sandy soil with heterogeneous layers of varying grain size distribution from fine sand to coarse gravel with stones. The top set unit is approximately 2 m thick and has horizontal beds of coarse sediments (gravel, gravely sand and medium to coarse sand). The underlying foreset beds are dipping and contain finer sediments, dominated by medium to fine sand. The whole area forms a flat plateau.

2.2. The experimental set-up

To avoid disturbing the snow profile above the ground surface, an electrolyte tracer was supplied as ice columns inserted under the snow cover on the ground surface along a line source (0.5 m wide) perpendicular to the lysimeter trench (Fig. 2). Five ice columns, 2.3 m long 6.86 cm in diameter, replaced the same volume of snow that had been removed near the ground surface. Thus, the tracer was supplied over the area monitored by both the suction cups and the ERT electrodes. The ice columns contained 1.86 g/l of NaBr, with a conductivity of 2.15 mS/cm. The tracer was supplied on 25 March 2001, prior to melting (usually late March–May). The air temperature was about -8°C . The tracer movement through the soil profile was observed using cross borehole ERT and suction cup lysimeter.

In the lysimeter trench, Teflon suction cup samplers (Prenart) are installed horizontally from the trench wall (French et al., 1994). They are positioned at regular intervals starting at a depth of 0.4 m down to 4.5 m. The distance from the wall to the suction cup increases from 0.7 m at 0.4 m depth to 1.1 m at 2.4 m depth. The filters have a pore size of $2\ \mu\text{m}$ and a porous area of $33\ \text{cm}^2$.

Two boreholes, labelled SEL2 and SEL3, situated

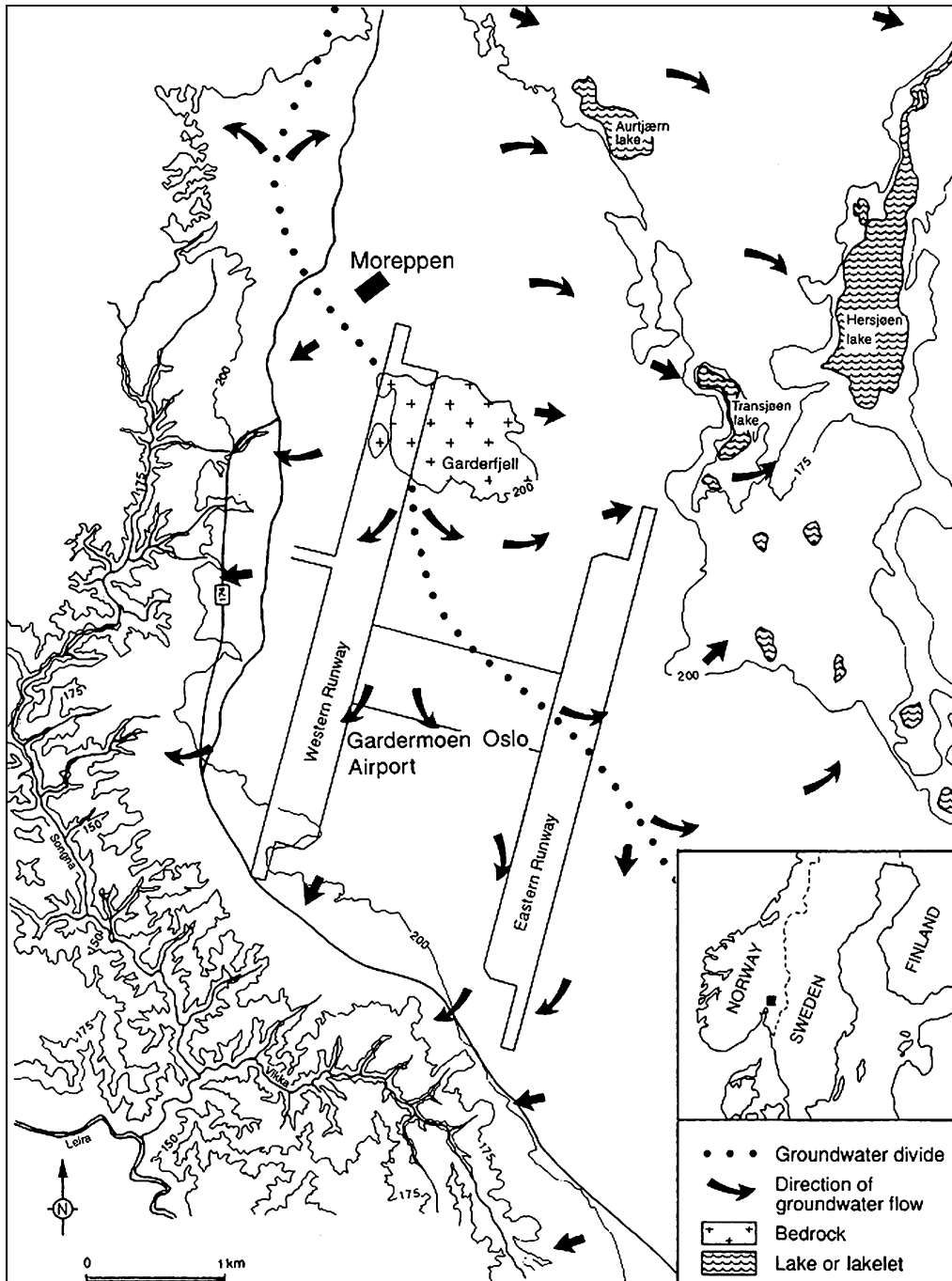


Fig. 1. Map of the Gardermoen delta including experimental field site, Moreppen, and area of Oslo airport.

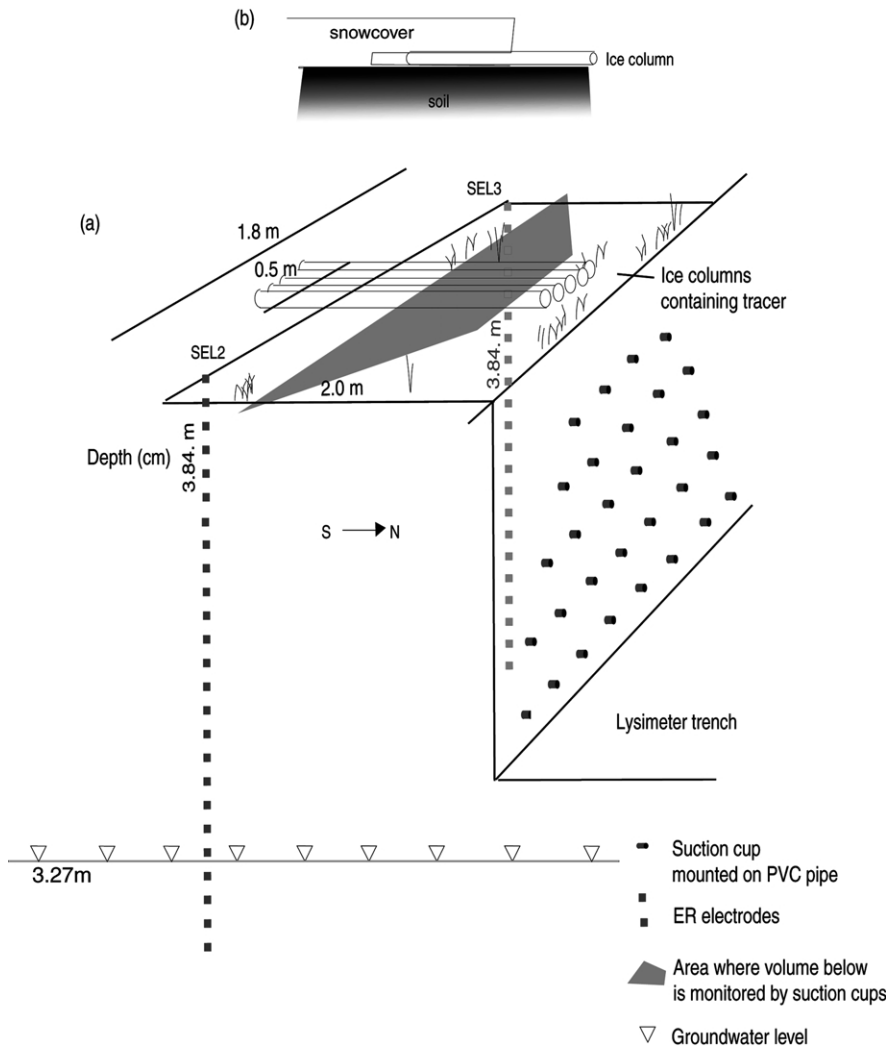


Fig. 2. (a) Schematic diagram of the lysimeter trench, including suction cups and boreholes containing electrodes. The ice columns are indicated on the surface as well as the area above the volume monitored by the suction cups. The distance from the wall to the suction cups increases from 70 cm at the top row to 110 cm at the bottom row. (b) Procedure for inserting ice columns under the snow cover.

1.8 m apart, were used for ERT data collection. Each borehole contained a set of 25 stainless steel mesh electrodes mounted, at 0.16 m intervals, on 4 cm diameter PVC pipes. The top electrode was situated near the surface, the bottom electrode at a depth of 3.84 m (Fig. 2).

2.3. Soil water sampling

Soil water samples were collected every second day. This included both point and integrated samples.

Point samples were collected approximately 3–4 h after the suction pump was set to 25 kPa. Integrated samples were left for a 2 day interval applying a suction of 15 kPa. All samples were then analysed for Br^- concentration using an Orion 9435 ion selective electrode and a double junction reference electrode. The sample electrical conductivity, as well as volume collected, was also measured. To support both the ERT and lysimeter data, soil temperatures were measured at depths ranging from 0.05 m down to 2.4 m in the north wall (Fig. 2). The height of the

water table was also automatically logged at hourly intervals with a Campbell CR10-based logger. A pressure sensor 6100BGN from Trans Instruments was calibrated for water level, accuracy ± 0.2 cm. Snow melting was monitored by measuring changes in snow depth (including water equivalents) and by collection of melt water from melting plates (French et al., 1999).

2.4. ERT data collection

Electrical resistivity data were collected from the time of tracer application on 25 March 2001 on a weekly basis until 7 May 2001. Thus, changes in the resistivity distribution, caused by the infiltration of both water and tracer, could be imaged as a function of time. The first data set was collected on 24 March prior to the onset of snowmelt and this was used as the background image.

A dipole–dipole configuration was used to collect the ERT data. In this configuration, current is applied to two adjacent electrodes and the resulting voltage between all remaining electrodes with the same spacing is measured. The smaller the distance between the current electrodes the more the current flow is biased towards the near-borehole region resulting in poor resolution at the centre (Slater et al., 2000). A small distance between potential electrodes gives a small voltage signal, resulting in a small signal-to-noise ratio (SNR) (Slater et al., 2000). By increasing the spacing of both the current and potential electrodes the resolution towards the centre of the profile and the SNR is improved. Preliminary inversions, using synthetic datasets based on resistivity estimates from preliminary trials carried out in January 2001, indicated that the optimal measurement scheme for the borehole arrangement is based on a current (and potential) electrode dipole separation of 0.48 m, i.e. three electrode spacings.

The dipole–dipole configuration described in previous sections, results in a total of 1172 resistance measurements. In order to assess data quality all measurements were repeated in a reciprocal dipole arrangement. Here, potential and current electrodes are swapped (Binley et al., 1995). Such an assessment permits removal of outliers prior to data inversion and also allows characterisation of data weights for the

inversion process. Collection of the complete set of 2344 measurements took approximately 10 h.

3. Data processing

3.1. ERT data inversion

To reduce the noise and to prevent misinterpretation of artefacts, measurements with reciprocity errors greater than 10% were removed from the data sets before inversion of the ERT data. A common measurement set for the whole time of the experiment was then selected, consisting of all measurements, which had acceptable reciprocity in all data sets. This ensured that image sensitivity was not biased by different measurements. Inversion of ERT data produces images of resistivity that should be consistent with the measured resistances. The procedure adopted here was the well established ‘Occams’ approach (LaBrecque et al., 1996). In this approach, the misfit between measured and theoretical resistances for a particular resistivity distribution is minimised whilst maintaining a smooth resistivity image.

The inversion was performed using a finite element based algorithm, which accounts for three-dimensional current flow in a two-dimensional resistivity field. A finite element grid consisting of 768 elements within the borehole plane was used and parameterised into 120 parameter blocks that lie between the two boreholes. Each ‘pixel’ has dimensions 0.125 m (horizontal) by 0.08 m (vertical) and is thus the resolution limit of the model (although this is reduced somewhat by the implicit smoothing of the algorithm).

Using the image produced from pre-tracer data collected on 24 March as a background (reference) state, images of changes in bulk electrical conductivity were produced to examine migration of the tracer and increased soil water content due to the snowmelt process.

3.2. Spatial moment analysis

Zero and first order spatial moments were calculated to evaluate and compare the plume development as monitored by ERT and suction cup measurements.

These moments give relatively robust descriptions of an irregular plume. Earlier studies, comparing calculations based on 30 nodes and 9000 nodes in a simulated domain, suggest that the first moment is well described by the 30 measurement points in this system (French et al., 2000). Direct measurements of Br^- concentrations from suction cups were used for the lysimeter data while changes in bulk conductivity values from the inversions were used for the ERT data. Spatial moments calculated from the two different field methods were based on measurements down to approximately 2.5 m.

The total mass of a non-sorbing solute in a two-dimensional vertical unsaturated profile, M_{00} , is described by:

$$M_{00}(t) = \int_{-\infty}^{+\infty} \int_{-\infty}^{+\infty} \varepsilon S_w(x, z, t) c(x, z, t) dx dz \quad (1)$$

where $c(x, z, t)$ is the concentration distribution field, S_w is the saturation, ε is the porosity, t is time and x, z are the spatial co-ordinates. Previous simulations assuming a constant εS_w , indicated little effect on the first and second moments, this is perhaps a rather crude simplification in periods where the soil is wetting up but we hope to attend to that in future experiments. However, as we had no detailed information about specific porosities and saturation levels at each point for this particular experiment the zero order moment in Eq. (1) was approximated by:

$$C_{00}(t) = \int_{-\infty}^{+\infty} \int_{-\infty}^{+\infty} c(x, z, t) dx dz \quad (2)$$

where $C_{00}(t)$ is the total concentration. The normalised zero order moment, $\tilde{C}_{00}(t)$ describes the recovery of solute ($C_{00}(t)$) relative to the input concentration ($C_{00}(t_0)$):

$$\tilde{C}_{00}(t) = C_{00}(t)/C_{00}(t_0) \quad (3)$$

The centre of mass of the plume is found by the first moment about the origin normalised by the zero order moment. The horizontal and vertical centres of mass, x_c and z_c , respectively, are given by:

$$C_{10}(t) = \int_{-\infty}^{+\infty} \int_{-\infty}^{+\infty} c(x, z, t) x dx dz, \quad (4a)$$

$$C_{01}(t) = \int_{-\infty}^{+\infty} \int_{-\infty}^{+\infty} c(x, z, t) z dx dz$$

$$x_c(t) = \frac{C_{10}(t)}{C_{00}(t)}, \quad z_c(t) = \frac{C_{01}(t)}{C_{00}(t)} \quad (4b)$$

A similar moment analysis may be performed on bulk conductivity changes observed from the ERT images.

4. Results and discussion

Fig. 3 shows the measured rainfall and snowmelt inputs measured during the period of ERT data collection. Also shown is the water table elevation change during the same period. The rapid rise in groundwater level following onset of snowmelt during early April illustrates the short response time of the system due to the highly permeable sediments.

In Fig. 4 the changes in subsurface temperature at three selected depths are shown. The stable thermal environment during the snowmelt period in April is clearly seen. Towards the end of April, a rapid increase in near surface temperature is apparent, with diurnal variation being clearly visible. The propagation of this elevated temperature with depth is also seen in Fig. 4. However, the stable conditions throughout most of the period of ERT data collection suggests that changes in groundwater conductivity due to temperature changes may not be significant.

4.1. Changes in Br concentration

In Fig. 5 images of Br^- concentration, interpolated using an inverse distance weighting procedure from measurements at the 28 sample locations, are shown with time. The images show the absolute bromide concentration for the interval 0.5–2.5 m depth.

During early April, little change is seen over the 0.5–2.5 m sampled region. A slight increase in concentration is observed at approximately 0.9 m depth to the left (Fig. 5a and b). By 15 April an increase in concentration is seen at 1.9 m depth (Fig. 5c) with no apparent increase in sample ports at shallower depths, indicating by-pass flow, possibly caused by heterogeneous infiltration and soil. High melt rates occurring over 1–2 days (Fig. 3) might also have some effect. By late April a more widespread increase in concentration is seen in the near surface sample ports and during early May the plume is seen to move vertically downwards at a steady rate. By 7

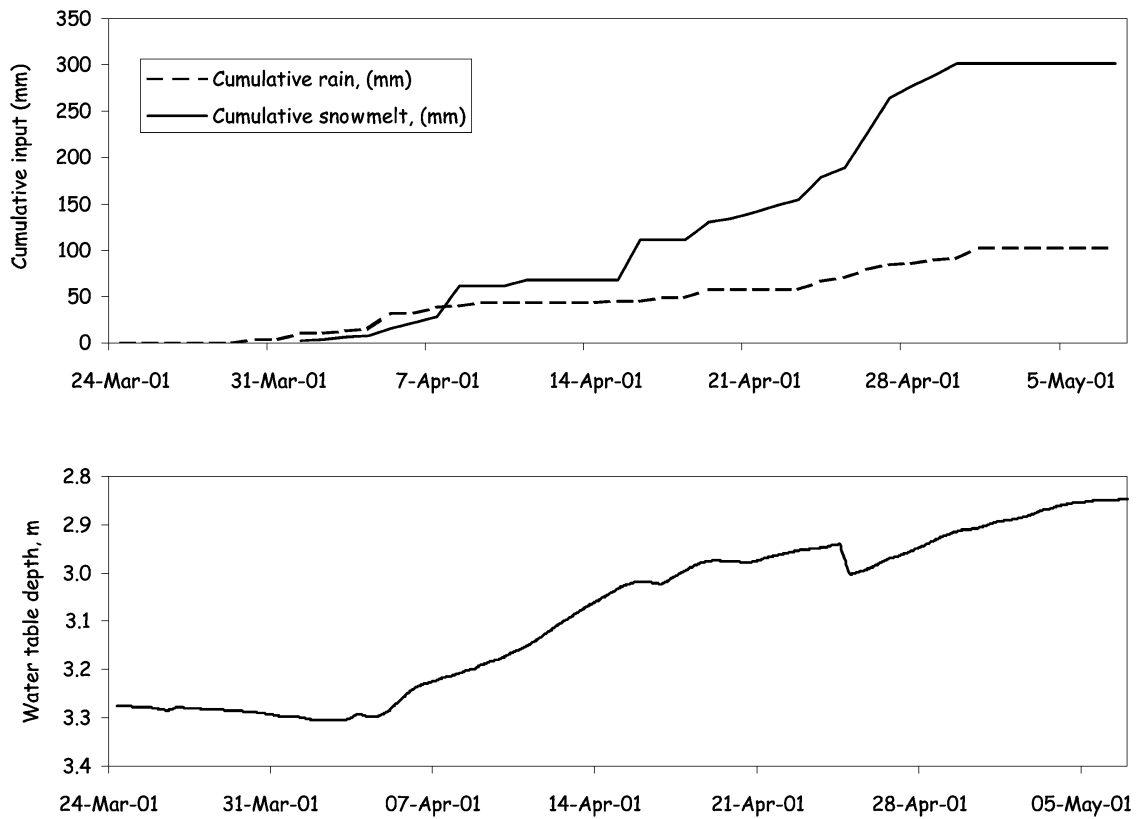


Fig. 3. Precipitation as rain and snowmelt versus time and observed changes in groundwater elevation.

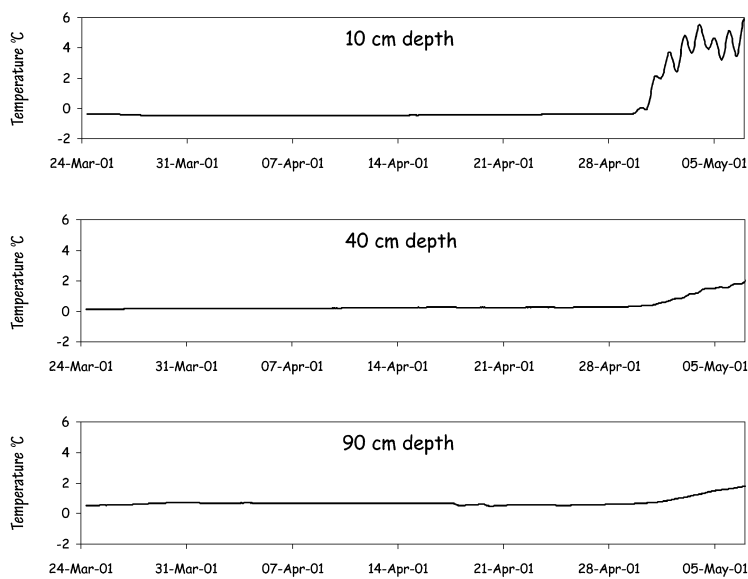


Fig. 4. Soil temperatures measured at depths 10, 40 and 90 cm during snow melting period of 2001.

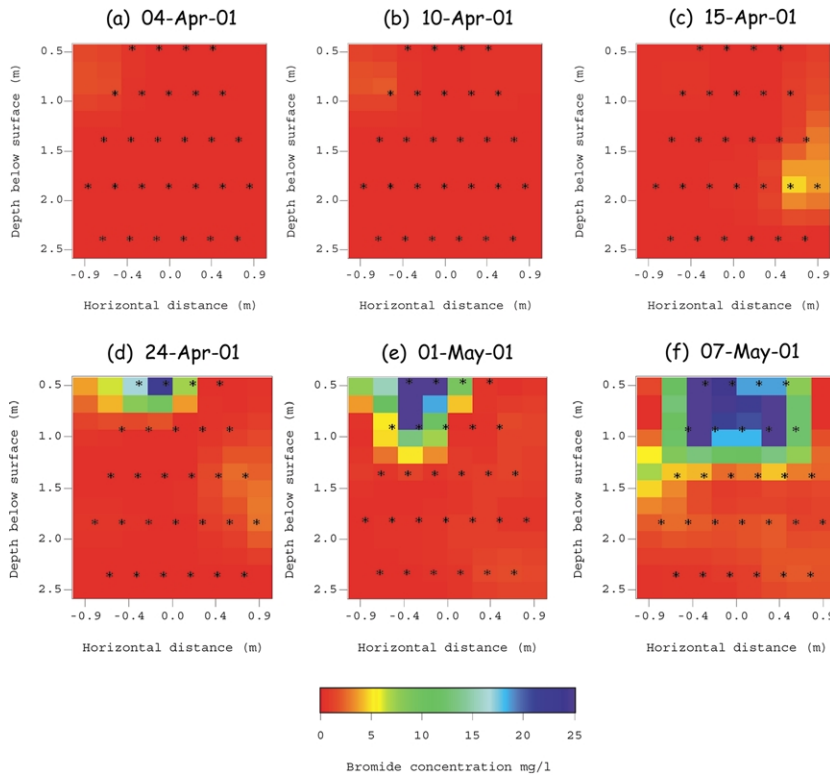


Fig. 5. Images of Br⁻ concentrations measured in suction cups during the period 4 April–7 May 2001. Approximate position of suction cup sample ports shown.

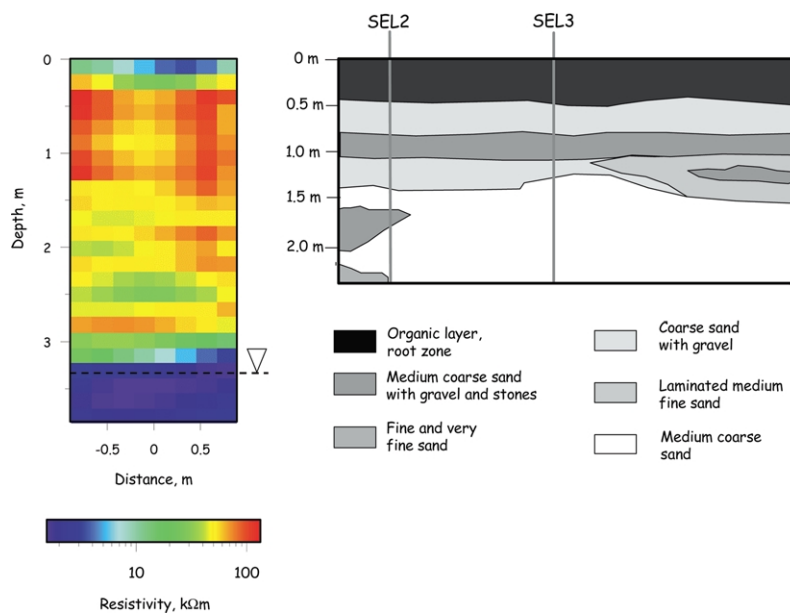


Fig. 6. Image of pre-tracer resistivity between SEL2 and SEL3 boreholes and observed lithology in southern wall of lysimeter trench. Position of water table is shown next to ERT image. ERT data collected 24 March 2001.

May the front of the plume has reached the sample ports at 1.4 m depth. Note also that the position of the Br^- plume front on 24 April and 1 May is to the left of the image plane. This supports the hypothesis that infiltration was uneven and that the plume development was affected by factors such as soil heterogeneity, basal ice or even soil frost.

4.2. Background ERT image

The pre-tracer ERT image, taken on 24 March confirms a similar soil structure as that found in the south wall of the trench (Fig. 6). The near surface soil horizon is relatively resistive, typically 3–30 k Ω m. This is due to a 0.2 m thick frozen layer (Fig. 4) and the well-drained nature of the sediments. The coarse sand and gravel layers between 0.5 and 1 m depth are revealed as a highly resistive zone with resistivities in the range of 50–200 k Ω m. As the measured subsurface temperatures at these depths are above 0 °C (Fig. 4) the observed high resistivity suggests a combination of very low moisture contents and low pore water conductivity. Measurements of electrical conductivity of pore water samples taken from various depths prior to the snowmelt period were in the range 20–30 $\mu\text{S}/\text{cm}$. Between 1.5 and 3.0 m depth, the resistivity is more varied, possibly indicating horizons of relatively lower permeability and higher moisture retention. Below 3.0 m the sharp drop in resistivity is caused by the water table (at approximately 3.3 m depth).

4.3. Change in ERT following tracer injection

The sequence of images in Fig. 7 show the changes in the conductivity distribution with time over the depth interval 0–2.5 m for dates corresponding with those for the Br^- concentrations in Fig. 5. Variation in conductivity at depths below 2.5 m is attributable to the water table rise shown in Fig. 3 and are thus of minor interest. The changes in bulk conductivity inferred from the ERT images are due to changes in moisture content and pore water conductivity. The latter will be mainly a result of transport of the NaBr tracer but also towards the end of the sequence as a consequence of elevated subsurface temperature.

The images suggest there is heterogeneity in the infiltration pattern, which appears to vary with time.

The tracer cores were placed centrally in the image plane and the first flush of melt water (Fig. 7a) looks to be evenly distributed. With the following images the infiltration pattern moves progressively to the left, suggesting non-uniform infiltration at the surface. It is only in the latter images, when the snow and soil frost has gone, that the pattern becomes more uniform. Such variation could indicate that ice lenses or inhomogeneous thawing of the soil influenced the infiltration pattern.

The changes in conductivity during April show a gradual increase towards the lower right of the image plane, suggesting preferred movement of water/tracer. This observation is consistent with the by-pass flow inferred from the Br^- concentration image on 15 April (Fig. 5c). A maximum change due to this effect occurs between 1.5 and 2.0 m depth towards the end of April (Fig. 7d). This effect becomes less pronounced, but perhaps leads to the localised increases at 2.5 m depth during early May. The most pronounced change in conductivity during early May (Fig. 7e) is the large increase in the depth interval 0.5–1.5 m. This appears to be the result of flushing of the tracer source due to thawing of the surface soils which, as shown in Fig. 4 occurs at this time. This is also supported by the more uniform distribution of larger conductivity values near the surface, as noted above. By 7 May the effect of this flushing is less pronounced (Fig. 7f). Again, the corresponding Br^- image (Fig. 5f) shows a similar pattern. Note also that the position of the Br^- plume front on 24 April and 1 May is to the left of the image plane, again showing a pattern consistent with the ERT images.

4.4. Spatial moments

In Section 4.3, the two field methods were compared visually on the basis of image interpretation. In this section, we examine whether it is possible to use spatial moments, calculated on the basis of absolute conductivity changes (from ERT), and on the basis of bromide concentrations measured in the lysimeter trench, as an objective method of comparison. Because of the various changes affecting the electrical resistivity during snowmelt, it is not straightforward to compare spatial moments based on the two methods. Changes in electrical conductivity are results of both changes in water content and

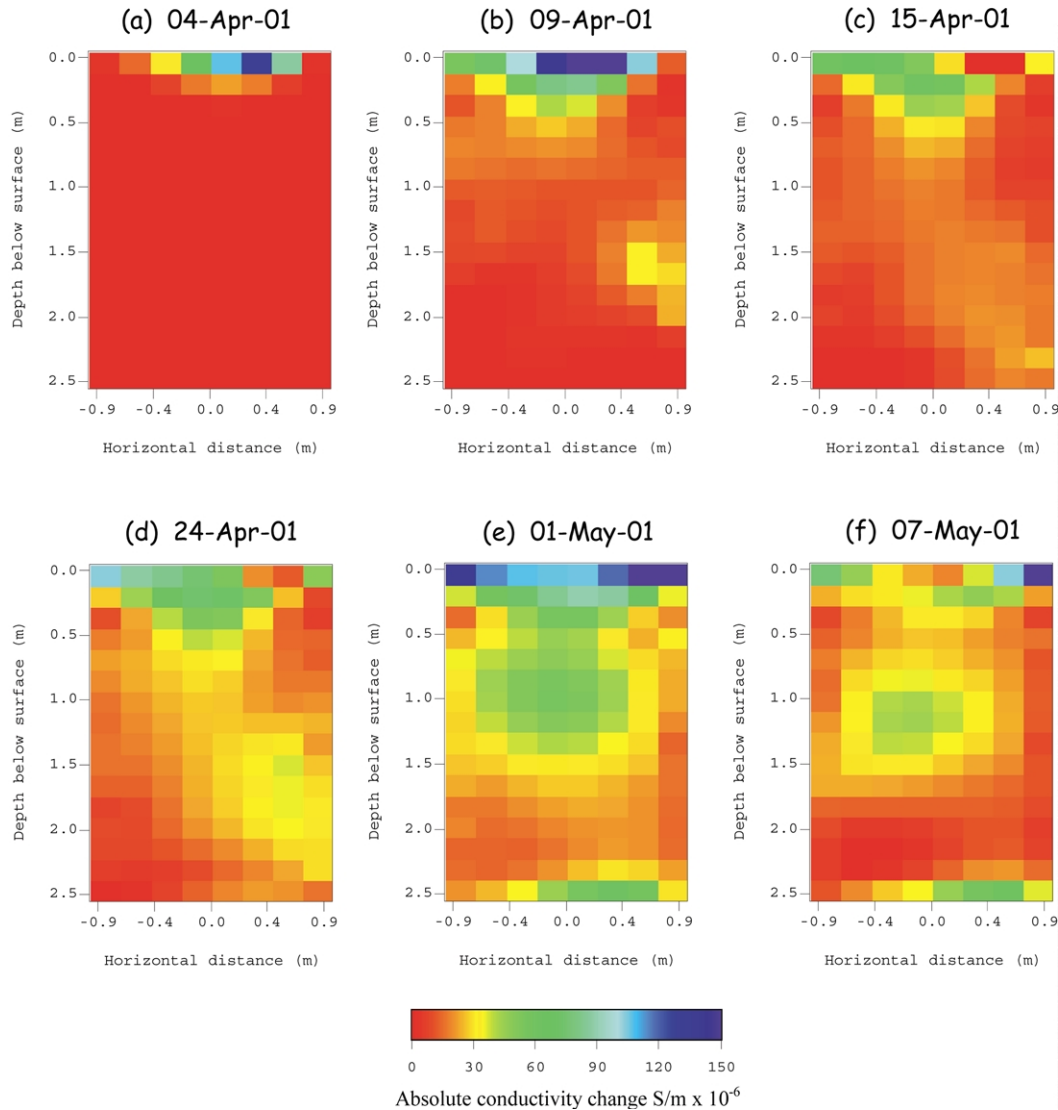


Fig. 7. ERT images showing change in bulk electrical conductivity between boreholes SEL2 and SEL3 using ERT data collected on 24 March 2001 as a reference.

concentration of ions in the soil water. Near the bottom of the profile monitored by the ERT set-up, resistivities were strongly affected by the rise in groundwater occurring during the snowmelt period. Thus, the ERT data set from 2.5 to 3.84 m depth was not included for this comparison. Spatial moment calculations based on ERT measurements were computed using all parameter cell values between the two boreholes in the top 2.5 m of the profile. For

the vertical profile monitored by suction cups, twenty-eight suction cups within the same domain as the ERT were used in the analysis.

Because of snowmelt input, the zero order moment for the Br^- concentrations shows a progressive increase during April and May, finally becoming steady during June and early July, followed by a steady decline as some of the Br^- is leached out of the monitored depth. The zero order moment for ERT

(total absolute change in conductivity) showed a maximum on 1 May (Fig. 8a). Since the change in conductivity is a function of increased water content and pore water ion concentration this maximum should indicate that most meltwater had infiltrated by this time, which corresponds well with observations of snow cover on the surface (Fig. 3).

The first order vertical spatial moments for the Br⁻ data show a two-stage process due to the initial by-pass flow, with an apparent transition during late April. The first order vertical spatial moments for ERT show the vertical migration of the wetting front and tracer plume. During early April a rapid change in the vertical spatial moment is seen and can be explained by the apparent preferential flow seen to depths of 1.5 m. By late-April the rate of change reduces, illustrating the slower migration of the bulk of the tracer, as in the case of the Br⁻ data.

The horizontal first order moments in Fig. 8c also show evidence of by-pass flow and heterogeneous infiltration. The horizontal centre of mass computed using the Br⁻ data initially moves from one side to the other because of the initially heterogeneous infiltration and flow pattern observed in the Br⁻ images. The horizontal moment based on the ERT images shows early movement off-centre due to the preferential flow. During the later stages the horizontal centre of mass remains near the centre of the monitored domain. The system is highly heterogeneous in all three directions within the layered structures. Earlier simulations of solute transport at the same site have suggested that randomly distributed permeability fields have captured the plume behaviour fairly well without including the layering structure (French et al., 1999).

5. Conclusions

An investigation of tracer transport under snow-melt conditions was performed at a site close to Oslo airport in Norway. Using cross-borehole ERT, images of changes in electrical conductivity were computed and compared to Br⁻ concentrations in pore water samples extracted from a number of suction cups installed in a lysimeter. The two methods show consistent results.

Both ERT and Bromide concentrations measured from 0.4 m downwards indicate the presence of

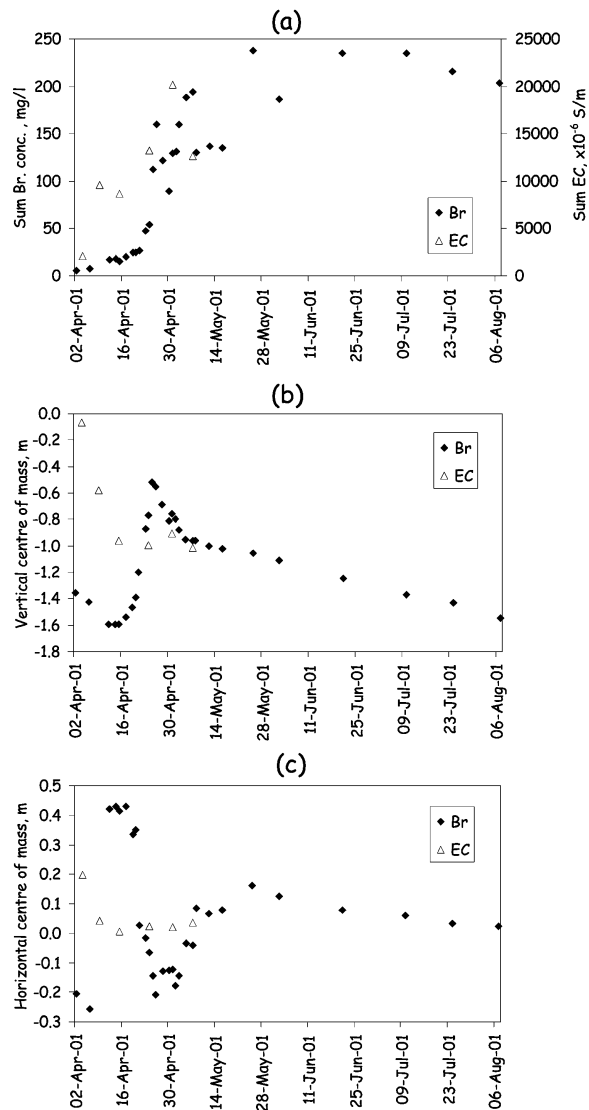


Fig. 8. Zero order (a), first order vertical (b) and first order horizontal (c) spatial moments versus time, calculated from ERT and Br⁻ data.

preferential flow paths during the early stages of the melting process. Later, when most of the Br⁻ has infiltrated more uniform flow prevails, as observed in previous experiments. Although there is a good agreement between the two methods, the ERT shows a more complete picture of changes in the water content through the whole profile, and the presence of preferential flow-paths during the early stages of the melting process. Both the heterogeneity

of the soil and the infiltration process seem to give rise to the initial heterogeneous flow pattern.

ERT would appear to be an appropriate tool for identifying zones of focused infiltration. Groundwater below these zones are most prone to pollution, localising them will therefore be of great value. Determining the area of focused infiltration will be useful in predicting tracer velocities in the unsaturated zone during snowmelt.

Acknowledgment

We would like to thank the Norwegian Research Council for supporting this work financially.

References

- Arcone, S.A., Sellmann, P.V., Delaney, A., 1979. Effects of Seasonal Changes and Ground Ice on Electromagnetic Surveys of Permafrost, USA CRREL Report, Cold Regions Research and Engineering.
- Binley, A., Ramirez, A., Daily, W., 1995. Regularised image reconstruction of noisy electrical resistance tomography data. In: Beck, M.S., Hoyle, B.S., Morris, M.A., Waterfall, R.C., Williams, R.A. (Eds.), *Process Tomography—1995, Proceedings of the Fourth Workshop of the European Concerted Action on Process Tomography*, Bergen, 6–8 April 1995, pp. 401–410.
- Daily, W., Ramirez, A., LaBrecque, D., Nitao, J., 1992. Electrical resistivity tomography of vadose water movement. *Water Resources Research* 28 (5), 429–1442.
- French, H.K., Swensen, B., Englund, J.-O., Meyer, K.-F., Van der Zee, S.E.A.T.M., 1994. A lysimeter trench for reactive pollutant transport studies. In: Soveri, J., Suokko, T. (Eds.), *Future Groundwater Resources at Risk*, vol. 222. IAHS Publication, Helsinki, Finland, pp. 131–138.
- French, H.K., Van der Zee, S.E.A.T.M., Leijnse, A., 1999. Differences in gravity dominated unsaturated flow during autumn rains and snowmelt. *Hydrological Processes* 13 (17), 2783–2800.
- French, H.K., Van der Zee, S.E.A.T.M., Leijnse, A., 2000. Prediction uncertainty of plume characteristics derived from a small number of measuring points. *Hydrogeology Journal* 8, 188–199.
- Jørgensen, P., Østmo, S.-R., 1990. Hydrogeology in the Romerike area, southern Norway. *Norges Geologiske Undersøkelse Bulletin* 418, 19–26.
- LaBrecque, D.J., Miletto, M., Daily, W., Ramirez, A., Owen, E., 1996. The effects of noise on Occam's inversion of resistivity tomography data. *Geophysics* 61, 538–548.
- Scott, W.J., Sellmann, P.V., Hunter, J.A., 1978. Geophysics in the study of permafrost. In: Ward, S.H., (Ed.), *Geotechnical and Environmental Geophysics*, Society of Exploration Geophysicists, pp. 355–384.
- Sinha, A.K., Stephens, L.E., 1983. Permafrost mapping over a drained lake by electromagnetic induction methods, current research, part A. Geological Survey of Canada, Paper 83 1A, 213–220.
- Slater, L., Binley, A., Daily, W., Johnson, R., 2000. Cross-hole electrical imaging of a controlled saline tracer injection. *Journal of Applied Geophysics* 44, 85–102.
- Stein, J., Kane, D., 1983. Monitoring unfrozen water content of soil and snow using time domain reflectometry. *Water Resources Research* 19 (6), 1573–1584.
- Todd, B.J., Dallimore, S.R., 1998. Electromagnetic and geological transect across permafrost terrain, Mackenzie River delta, Canada. *Geophysics* 63 (6), 1914–1924.
- Tuttle, K., 1997. Sedimentological and hydrogeological characterisation of a raised ice-contact delta—the preboreal delta-complex at Gardermoen, Southeastern Norway. PhD Thesis, Department of Geology, University of Oslo.